

A Review of X-ray Observations of Supernova Remnants

Jacco Vink ^{a b *}

^aColumbia Astrophysics Laboratory, Columbia University, New York, NY, USA

^bPresent address: SRON National Institute for Space Research, Sorbonnelaan 2, 3584 CA Utrecht, Netherlands

I present a review of X-ray observations of supernova remnants with an emphasis on shell-type remnants. The topics discussed are the observation of fresh nucleosynthesis products, shock heating and cosmic ray acceleration.

1. INTRODUCTION

Although radio and optical observations have played an important role in identifying and characterizing supernova remnants (SNRs), most of the shock heated material is primarily visible in X-rays, having temperatures of typically $10^6 - 10^7$ K. The emission mechanisms are bremsstrahlung and line radiation, but a number of remnants are now known to emit X-ray synchrotron radiation from ultra-relativistic electrons, as well. This was already known for pulsar wind nebula dominated, or Crab-like remnants, which fall outside the scope of this review, but also shell-type remnants like SN 1006 emit synchrotron radiation from electrons accelerated by the blast wave [1].

The X-ray line emission of SNRs is in particular interesting, as it allows the study of the most abundant metals, the so called α -elements, which prominently feature in the X-ray spectra of young SNRs like Cas A, Tycho (SN 1576) and Kepler (SN 1064). This line emission, and mass estimates based on the X-ray emission, give important information on the nucleosynthesis yields of the explosions, which can then be compared to theoretical supernova (SN) models [2,3].

The line and bremsstrahlung emission give us a window on the past of the SNR: its progenitor and the SN explosion. X-ray synchrotron radiation, on the other hand, is interesting as it provides a window on cosmic ray shock acceleration. SNRs are thought to be the primary source of cosmic rays up to, and possibly beyond, energies of $10^{15.5}$ eV, at which energy the spectrum has a break, usually referred to as "the knee". However, direct evidence for a SNR origin for cosmic ray particles other than electrons is lack-

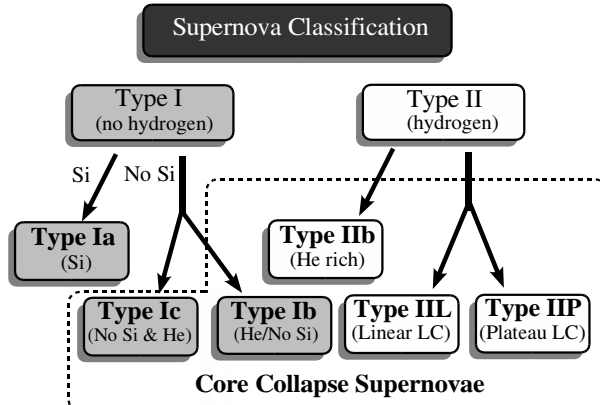


Figure 1. The supernova classification scheme, which is based on optical spectroscopy and light curve (LC) shape.

ing. For a long time the observational support for a SNR origin of cosmic rays was the detection of radio synchrotron emission from SNRs, revealing the presence of cosmic ray electrons up to energies of a few GeV. Recently the detection of X-ray synchrotron radiation from SNRs have substantially extended this to ~ 100 TeV [1,4].

In this review I will discuss recent findings concerning both the study of fresh nucleosynthesis and cosmic ray acceleration in SNRs, emphasizing the role of X-ray observations, including results based on *BeppeSAX* observations.

*Chandra fellow

2. SUPERNOVA REMNANTS AND THEIR PROGENITORS

Two recent astrophysical developments have boosted the interest in supernovae (SNe): the use of Type Ia SNe as standard candles to study the geometry of the Universe (e.g. [5]), and the discovery that gamma-ray bursts (GRBs) may be associated with Type Ib/c SNe (e.g. [6]).

Type Ia and Type Ib/c SNe are very different objects (see Fig. 1): Type Ia SNe are probably caused by the thermonuclear disruption of a C-O white dwarf following mass accretion, but the nature of the binary system, nor the disruption mechanism (detonation, deflagration, delayed detonation) are yet known [7]. Type Ib/c and Type II SNe, on the other hand, are core collapse SNe of massive stars, i.e. $> 8 M_{\odot}$ while on the main sequence (MS). The classification is for historical reasons confusing. Only since two decades are Type Ib/c recognized as a special subclass, like Type Ia their optical spectra show no H absorption, but for Type Ibc the likely reason is the loss of the hydrogen envelope of a massive star, either due to binary mass transfer or due to a strong stellar wind.

The energy source for the explosion of core collapse SNe is the gravitational collapse of the stellar core. The stellar core itself will leave a neutron star or black hole behind, and the energy for the explosion comes from the release of gravitational binding energy. The energy is primarily released in the form of neutrinos, but to order 1% is kinetic energy. The SN-GRB connection has led to a new interest in the explosion mechanism itself. A large fraction of the GRB energy must be in the form of jets, and a natural question then is how these jets are formed and whether jet-formation plays a role in the explosion of core-collapse SNe in general.

2.1. Core collapse remnants

Both core-collapse and Type Ia SNe release $\sim 10^{51}$ erg in kinetic energy. It is therefore sometimes difficult to distinguish remnants from both types of explosions. However, the presence of a pulsar clearly identifies a remnant as a core collapse remnant. In other cases we have to rely on abundance patterns, if relatively unmixed ejecta are present, and circumstantial evidence such as the proximity of an OB association. Clearly identifiable ejecta are found in young

remnants, but have also been found in SNRs of several thousand years old; e.g. the fast moving ejecta fragments associated with the Vela remnant [8], or Si-rich, X-ray emitting material from the center of the Cygnus Loop [9].

Younger remnants are useful to obtain a more complete understanding of nucleosynthesis yields. Especially the so called O-rich SNRs are important, as they are likely to be remnants of the most massive stars, which have a higher O yield. These remnants are therefore possibly remnants of Type Ib/c SNe. Among them are the young SNRs Cas A, G292.0+1.8 (MSH11-54) and E0102-7219 (Fig. 2). Initially their identification as O-rich was based on optical line emission, but X-ray spectroscopy confirms that they are O-rich. Interestingly, although they are probably remnants of very massive stars, which are thought to produce black holes rather than neutron stars [10], G292.0+1.8 harbors a 135 ms pulsar [11] and Cas A a neutron star candidate in the form of a non-pulsating point source, similar to another O-rich remnant, Puppis A [12]. Cas A may have been a 18-25 M_{\odot} MS star, consistent with the presence of a neutron star, but a recent analysis of *Chandra* data of G292.0+1.8 led [13] to the conclusion that it is the remnant of a 30-40 M_{\odot} MS star, which according to [10] should have produced a black hole.

Cas A is the youngest galactic remnant, and one of the best studied ones ([14], for a review). It is also the remnant that was observed very extensively with *BeppoSAX* [15,16,17,18,19]. One remarkable feature observed with *BeppoSAX* was the fact that the Fe-K line emission peaked in the southeast, outside the main Si-rich ejecta shell [16]. *Chandra* has revealed that the Fe-K emission is not coming from shock heated circumstellar material, but from Fe-rich ejecta knots [20]. This is quite remarkable, because, according to standard SN models, the Fe-rich shell lies inside the Si and O-rich shells. Some of the knots seem to be almost pure Fe, and have been identified as α -rich freeze-out products [21]. This process arises if during the explosion very hot material, 5×10^9 K, rapidly expands. In the northern part of Cas A other Fe-rich material is found inside the main shell, but an X-ray Doppler study, based on *XMM-Newton* observations, reveals that the Fe in this region is moving faster than Si and S. The position of Fe inside the northern shell is therefore likely to be a projection effect [22].

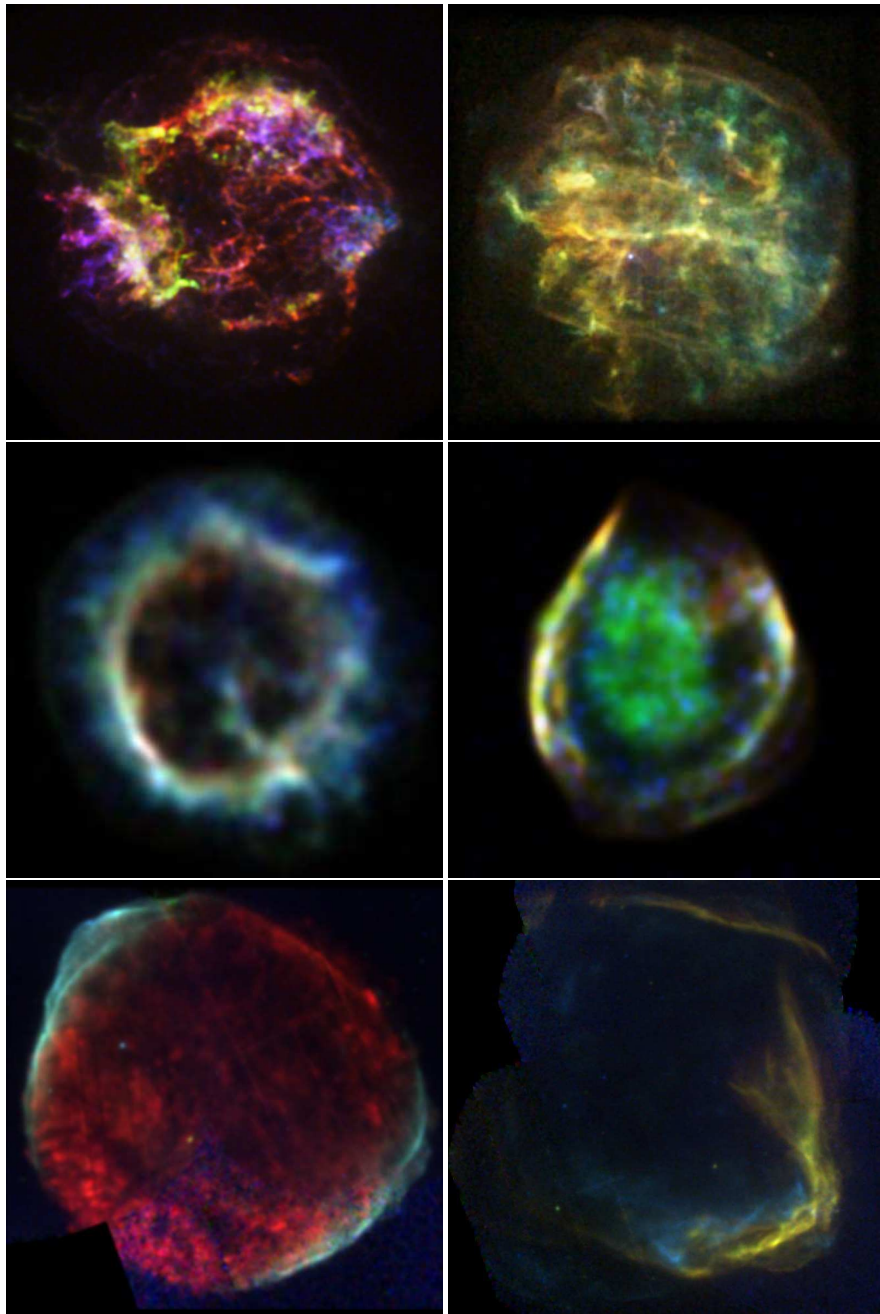


Figure 2. *Chandra* and *XMM-Newton* (bottom images) images of supernova remnants. From left to right, top to bottom: Cas A (Mg XII, Si XIII), G292.2-1.8 (OVII/VIII, Ne, Si XIII), E0102-7219 (OVII, OVIII, Ne/Mg), Dem L71 (O,Fe L, Si), SN 1006 (O VII, 0.7-2 keV, 2-7 keV), and RCW 86 (O VII, 0.7-2 keV, 2-7 keV). The labels in parenthesis refer to the energy bands used for the RGB colors.

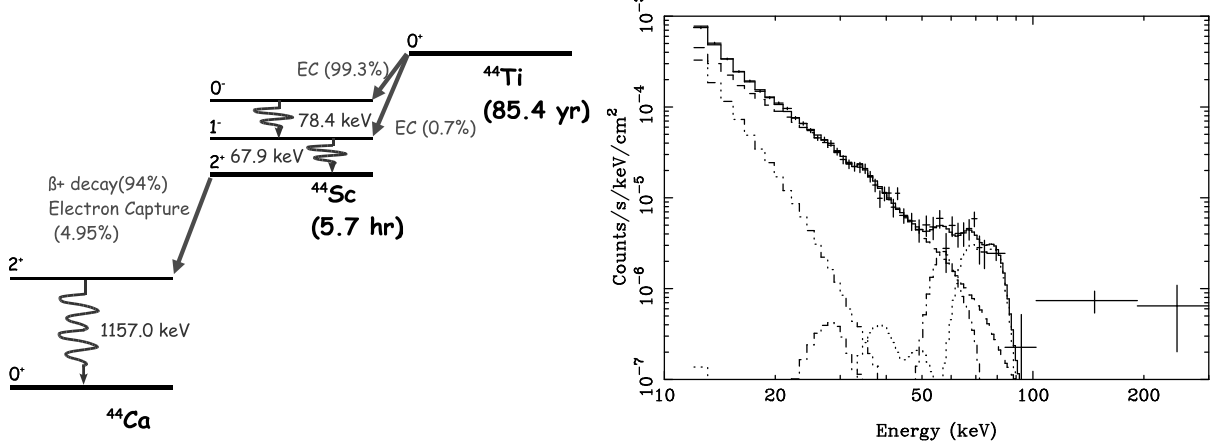


Figure 3. The decay scheme of ^{44}Ti (left) and the *BeppoSAX*-PDS spectrum of Cas A, showing the presence of the 68 keV and 78 keV (^{44}Sc) decay lines (right). The various contributions to the spectrum are indicated separately, the dotted line indicating the ^{44}Sc contribution. The low level components between 20-60 keV is instrumental (escape peaks of the line emission).

The *XMM-Newton* study also confirms the large deviations from spherical symmetry in the expansion of Si, S and Fe, with the southeastern part having a bulk redshift and the northern part a bulk blueshift. The asymmetries are likely due to explosion asymmetries in the kinematics of the ejecta from the core as the forward shock, which is more indicative of the circumstellar medium and is marked by a narrow X-ray synchrotron emitting filament [23], is remarkably circular. An aspherical ejecta expansion has also been found for the SMC O-rich SNR E0102-7219 with *Chandra*-HETG high resolution spectroscopy [24].

Keeping in mind the GRB jets, one may wonder whether the asymmetries in these likely Type Ib systems are related to the asymmetries in the much more energetic GRBs. Cas A has an interesting jet-like structure in the northeast, with a possible weaker counterpart in the west [14]. However, it consists of Si-rich material, and is therefore unlikely to have formed close to the collapsing core. The Fe-rich core material on the other hand is clearly aspherical, but its kinematics do not reveal any bipolarity. This is not necessarily in disagreement with a scenario in which a SN explodes with a collapsar-like mechanism, i.e. an accretion powered SN, because collapsar models

show that ^{56}Ni , which decays to Fe, is not produced in the jets but in a “wind” in between the jets and the accretion disk [25]. On the other hand the latest numerical simulations of a conventional core collapse also indicates the formation of high velocity Ni-rich material [26].

^{56}Ni nucleosynthesis in an environment in which the density drops rapidly due to expansion gives rise to α -rich freeze out [27]. The synthesis of radioactive ^{44}Ti is a very characteristic byproduct of this process. ^{44}Ti decays in ~ 85 yr into ^{44}Sc , which decays to ^{44}Ca (Fig. 3). Interestingly, Cas A is one of only two objects in which ^{44}Ti has been detected [28,29]. The characteristic ^{44}Ca at 1157 keV was detected by *CGRO-Comptel* [28] with a flux of $7 \times 10^{-5} \text{ ph cm}^{-2}\text{s}^{-1}$. For some time, however, this detection was not consistent with the non-detection of the ^{44}Sc lines at 68 keV and 78 keV by *CGRO-OSSE* and the high energy experiments on board *RXTE*, and *BeppoSAX* [30,31,17]. Finally, however, a 500 ks *BeppoSAX* observation of Cas A resulted in a better than 3σ detection of those lines (Fig. 3) [19,32] with a flux of $(3.3 \pm 0.3) \times 10^{-5} \text{ ph cm}^{-2}\text{s}^{-1}$, with some uncertainty due to the uncertain shape of the hard X-ray continuum. Assuming an age for Cas A of 320 yr

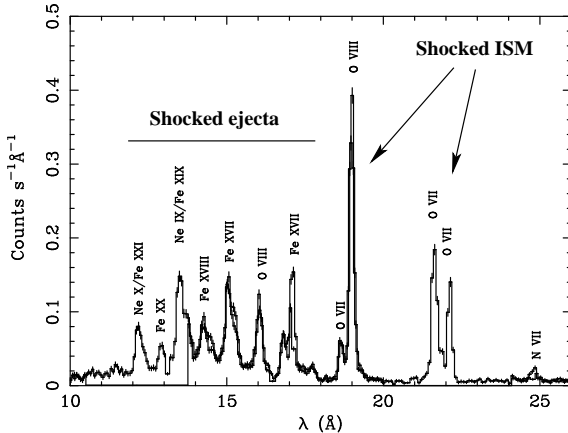


Figure 4. The high resolution *XMM-Newton* RGS spectrum of Dem L71 [38].

and a distance of 3.4 kpc [33], the combined *CGRO-Comptel* and *BeppoSAX* detections translate into an initial ^{44}Ti mass of $(1.8 \pm 0.3) \times 10^{-4} \text{ M}_\odot$. This is higher than expected based on the standard nucleosynthesis models [2], but consistent with either large scale explosion asymmetries or a higher explosion energy (2×10^{51} erg instead of 10^{51} erg, see also [34]). The detection of ^{44}Ti , together with reasonably reliable yields of other elements [35,36], make Cas A one of the best examples of how X-rays helps us to form a better picture of core collapse SNe.

2.2. Type Ia remnants

In order for a C-O white dwarf to be disrupted and eject material with a high velocity more than 0.5 M_\odot of C-O has to be burned into ^{56}Ni . One can therefore expect that young Type Ia SNRs copiously emit Fe line emission, either Fe-L emission in the energy range from 0.8-1.2 keV (Fig. 4), or Fe-K emission from 6.4-7 keV.

The Fe-L emission consists of many lines giving rise to a bump in X-ray spectra observed with CCD detectors such as found on *ASCA*, *XMM-Newton*, and *Chandra*. In [39] it was observed that LMC remnants fall into two classes, those with prominent Fe-L emission and those without. The Fe-L dominated remnants are likely Type Ia remnants. However, one

should be careful in applying this method. For example, Kepler's remnant would be accepted as a Type Ia remnant, whereas optical spectroscopy of Kepler shows the presence of N overabundance suggesting a core collapse remnant [40]. Another example is SNR Tycho (SN 1572), which is generally accepted to be a Type Ia remnant, but it lacks prominent Fe-L emission. However, Tycho's X-ray spectrum does show Fe-K emission, which peaks at a smaller radius than the spectral lines of other elements. This clearly indicates that there is an elemental stratification, just as expected for Type Ia remnants, with an inner ejecta layer consisting of Fe and the outer ejecta of mid-Z elements [41,42]. The lack of Fe-L emission from Tycho can be attributed to the low ionization age of the plasma.²

A similar lack of Fe-L emission from another historical Type Ia remnant, SN 1006 (Fig. 2), can also be attributed to the low ionization age of $n_e t \sim 2 \times 10^9 \text{ cm}^{-3}\text{s}$ [16,43,44]. An overabundance of Fe was reported in [43] and [44] but high resolution spectroscopy with the *XMM-Newton* RGS instruments did not reveal any signatures of Fe-L emission [45]. Abundance determinations for SN 1006 of O, Ne, Mg, and Si are more reliable, as those lines are clearly visible in CCD spectra. So any low spectral resolution X-ray Fe abundance measurements of SN 1006 should be regarded with caution, especially since Fe is in an ionization stage (< Fe XVII), which produces almost no Fe-L emission. Another reason to distrust Fe abundance measurements in SN 1006 is that optical absorption spectra toward a bright UV background star reveals that the reverse shock has probably not yet reached the Fe-rich ejecta [46]. SN 1006 is in that sense both dynamically and spectroscopically younger than Tycho's remnant, a result of its evolution in a low density environment.

In order to see all Fe one has to observe dynamically older remnants, in which the reverse shock has heated almost all ejecta. A good example is Dem L71 [37]. *Chandra* images in the energy bands of O and Fe-L show that most of the O VII/VIII emission comes from a narrow shell, but most Fe-L line emission comes from the center of the remnant (green in Fig. 2, see also Fig. 4). In fact, assuming that the

²SNR plasmas are often out of ionization equilibrium, due to a combination of a low electron density, n_e , and a short time, t , since the plasma was heated.

plasma inside the shell consists of pure Fe, the estimated Fe mass is $\sim 0.8 M_{\odot}$ [37,38], consistent with Type Ia nucleosynthesis models [3]. In general, assuming that a plasma consists of a pure metal plasma, with no or little H, will give rise to a lower overall mass estimate and a higher mass estimate for that particular metal. Critical to this calculation is the source of the exciting electrons. Although, most of the Fe ejecta seems to be shocked, Dem L71 is less suitable for obtaining the overall ejecta abundances, as the outer C-O, and Si layers are likely to be mixed with the ISM. Therefore, advances in our understanding of Type Ia SNe should probably come from combining studies of young and old Type Ia remnants.

3. SUPERNOVA REMNANTS AND COLLISIONLESS SHOCK PHYSICS

Supernovae drive shock waves through the ISM that remain visible for 10,000's of years in the form of SNRs. As the ISM is very tenuous, the particle mean free path is larger than the typical shock width. That a shock forms at all is due to the fact that heating occurs not through two body interaction, but due to the coupling of particles with self-generated plasma waves. These so-called collisionless shocks are interesting from a physical point of view, since the detailed shock heating process is unknown, and the process can only be studied in the rarefied media in space.

3.1. Shock heating

One question considering collisionless shocks is whether they heat each particle species according to its own Rankine-Hugoniot equation³, or whether different particles are quickly equilibrated by the collisionless heating process (i.e. $kT_e = kT_H = kT_{He}$, etc.). The first evidence for non-equilibration of temperatures was that UV line emission from SN 1006 indicates that H, C, and O have approximately the same line width, instead of a line width inversely proportional to the particle mass, as can be expected for an equilibrated shock [47]. Other evidence came from modeling the width of H α line emission in comparison with the narrow to broad line H α ratio observed in a number of SNRs, which seem to indicate that low Mach number shocks are fully equilibrated, whereas

³ $kT_i = 3/16m_i v_s^2$, for high Mach number shocks and species i , without additional energy sinks, such as CR acceleration.

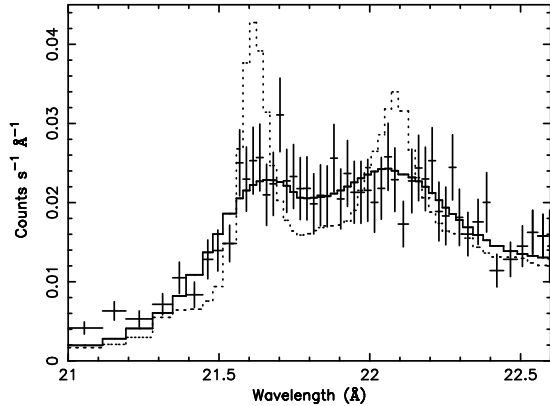


Figure 5. *XMM-Newton* RGS high resolution spectrum of the bright compact knot at the northwestern edge of the remnant. The dotted line shows the best emission model excluding, the solid line including thermal Doppler broadening [45].

high Mach number shocks are not [48]. A recent measurement of the O VII line widths of a compact knot in SN 1006 indicate a high O VII temperature of $\sim 350 - 700$ keV compared to an electron temperature of ~ 1.5 keV (Fig. 5, 2) [45].

A remaining question is whether the shock heating process does always produce a Maxwellian particle distribution and what the influence is of cosmic ray acceleration on the temperature(s), as cosmic rays provide an additional heat sink, or even lead to heat loss as a result of CR escape. This process may have been observed in E0102-7219, which showed an electron temperature too cold compared to the observed expansion velocity, even if the non-equilibration of electron and proton temperature was taken into account [49].

3.2. Particle acceleration

SNRs are considered to be the dominant source of cosmic rays up to the “knee”. The reason is that the likely galactic SN rate of 1-2 per century is sufficient to maintain the observed cosmic ray density in the galaxy, provided that up to 10% of the available SN kinetic energy is used to accelerate particles. The energetic cosmic rays observed on earth

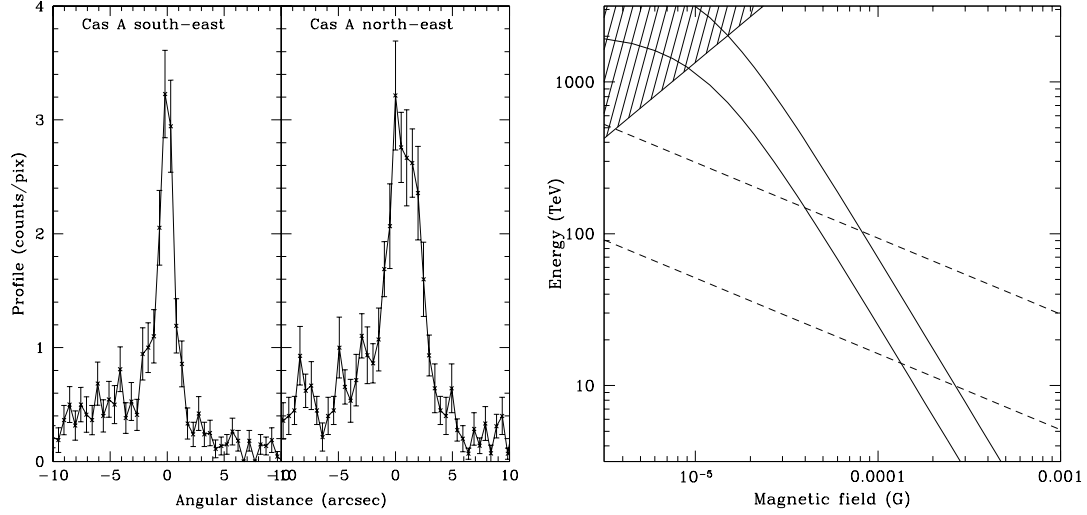


Figure 6. Left: Profiles across Cas A’s continuum rims (*Chandra* data). The widths can be converted to a combination of magnetic field (B) and electron energy (E), assuming that the width is determined by synchrotron losses (curved lines, right). Together with the observed photon energy (straight lines) this gives approximate E and B estimates (after [32]).

are primarily nuclear cosmic rays, unfortunately observations of SNRs lead primarily to the detection of electron cosmic rays due to synchrotron or inverse Compton radiation. In principle, nuclear cosmic rays can be detected, as collisions of energetic heavy particles with background matter leads to the production of pions. The neutral pions decay emitting two photons, which can be detected by gamma-ray satellites such as the future GLAST mission or by TeV Čerenkov telescopes. Several SNRs, such as SN 1006[50], Cas A [51], and RXJ 1713.7-3946[52], have been detected with Čerenkov telescopes, but it is not clear whether the observed emission is due to inverse Compton emission from electrons or pion decay due to nuclear cosmic rays.

The recent discovery of X-ray synchrotron emission from a number of SNRs, SN 1006⁴ [1,53,43], Cas A [32], RCW 86 [54], RXJ 1713.7-3946[55,56], and G266.2-1.2 (“Vela jr”) [57], have extended the observed electron energies from the GeV range (from radio observations) to 10-100 TeV energies. Although

this is additional proof that electrons are accelerated to high energies, the observed energy range falls short of the “knee” energy [4]. Interestingly this list includes all remnants detected at TeV energies.

The identification of the TeV emission as either pion decay or inverse Compton radiation depends on the magnetic field strength, which is needed to convert the observed X-ray photon energies into electron energies. This dependency can be used to infer the magnetic field strength assuming that the TeV emission is inverse Compton radiation [43], or, if a field strength is estimated, to identify the nature of the TeV emission [58].

One usually assumes that the post shock magnetic field strength is compressed by the shock and is at most a factor 4 times the canonical galactic field value of $B \sim 5 \mu\text{G}$. However, the spatial resolution of *Chandra* has lead to resolving the narrow X-ray synchrotron structures at the shock fronts of Cas A and SN 1006 [32,59], from which one can infer the interior magnetic fields close to the shock front, if one has an estimate of the shock velocity [60,61], as illustrated in Fig. 6. For both remnants the post shock

⁴See the green-blueish color in the *XMM-Newton* image of SN 1006, Fig. 2 bottom left.

magnetic field turns out to be around $100 \mu\text{G}$ [32,62]. If correct this would mean that the TeV gamma-ray emission from SN 1006 is due to pion decay [58], whereas for Cas A pion decay is likely, but inverse Compton emission cannot be excluded [32].

The large magnetic fields found in Cas A and SN 1006 provide additional support for the idea that SNRs can accelerate nucleons up to the “knee” energy, as the X-ray observations indicate that the electron maximum energy is bound by synchrotron losses, not by acceleration time. If the latter were the case then the maximum nucleon energy would be comparable to the maximum electron energy, i.e. $< 100 \text{ TeV}$. A higher magnetic field allows for the possibility that nucleons are accelerated to higher energies, and, moreover, higher magnetic fields increase the acceleration efficiency.

The detection of X-ray synchrotron emission from shell-type SNR has advanced our knowledge of cosmic ray acceleration. However, one should approach its detection with some caution. So far the identification of X-ray synchrotron emission has been based on a power law continuum shape, and the (near) absence of (thermal) line emission. For Cas A the detection of X-ray synchrotron emission was based on the presence of hard X-ray continuum [65]. Its nature is, however uncertain. *XMM-Newton* images of emission around 10 keV show that emission is still coming from the interior of Cas A, whereas one does not expect X-ray synchrotron emission from the inside, as synchrotron losses due to the high interior magnetic field of $> 0.5 \text{ mG}$ [32] make it unlikely that a very energetic electron population can be maintained. An alternative mechanism for the X-ray continuum in terms of non-thermal bremsstrahlung from electrons accelerated by lower hybrid waves has been proposed [66] and model spectra fit the *BeppoSAX* data well [32] (Fig. 3). Also for the hard X-ray emission from IC 443 has a non-thermal bremsstrahlung origin been proposed [67,68]. This emission may arise from an interaction of the SNR with molecular clouds or from fast moving ejecta fragments [69].

Another case where there has been a controversy about the nature of the X-ray continuum emission concerns the X-ray continuum from RCW 86, a $40'$ sized SNR (Fig. 2). *ASCA* and *BeppoSAX* data showed that the soft X-ray emission, dominated by line emission, has a very different morphology than

the continuum emission, which manifests itself most clearly above 2 keV [63,67] (Fig. 2). This was taken as evidence for X-ray synchrotron emission [70], in analogy with SN 1006. However, the hard X-ray continuum is not entirely featureless, since Fe-K line emission has been solidly detected and seems to come from the hard X-ray emitting regions. So an alternative theory for the hard X-ray emission is that it is due to (non-thermal) bremsstrahlung from electrons with energies up to 100 keV , which are also responsible for the Fe-K emission [63,64]. Additional evidence for questioning the synchrotron hypothesis is the lack of radio synchrotron emission from hard X-ray producing regions (Fig. 7). The Fe-K emission has an energy of 6.4 keV , indicating that it is caused by low ionization stages of Fe, i.e. either from a cold or a severely underionized plasma. The problem with the bremsstrahlung hypothesis is that the presence of the bremsstrahlung producing electrons has to heat up the background material, which should manifest itself in line emission of O VII [54]. The synchrotron hypothesis, on the other hand, needs the presence of an additional hot, but very underionized pure Fe plasma, in order to explain the Fe-K emission [54]. This debate will be helped by deeper *Chandra* and *XMM-Newton* observations. Especially observing the spatial morphology in Fe-K emission is important, because the bremsstrahlung hypothesis predicts a morphology similar to the continuum emission, and the synchrotron plus hot pure Fe hypothesis predicts patches of Fe-K emission and spatially uncorrelated, diffuse X-ray continuum emission.

Whatever the outcome it will either give new insights in the acceleration of electrons at the low end, or at the high end of the electron cosmic ray spectrum. Moreover, if the Fe-K is indeed from pure Fe this may have interesting consequences for our understanding of RCW 86’s progenitor.

4. Concluding remarks

The last paragraph shows that to some extent the issue of cosmic ray acceleration and explosive nucleosynthesis are intertwined. In order to assess abundance patterns an understanding of the radiation processes, bremsstrahlung, line emission, and synchrotron emission is needed. The possible presence of synchrotron emission in a line dominated spectrum

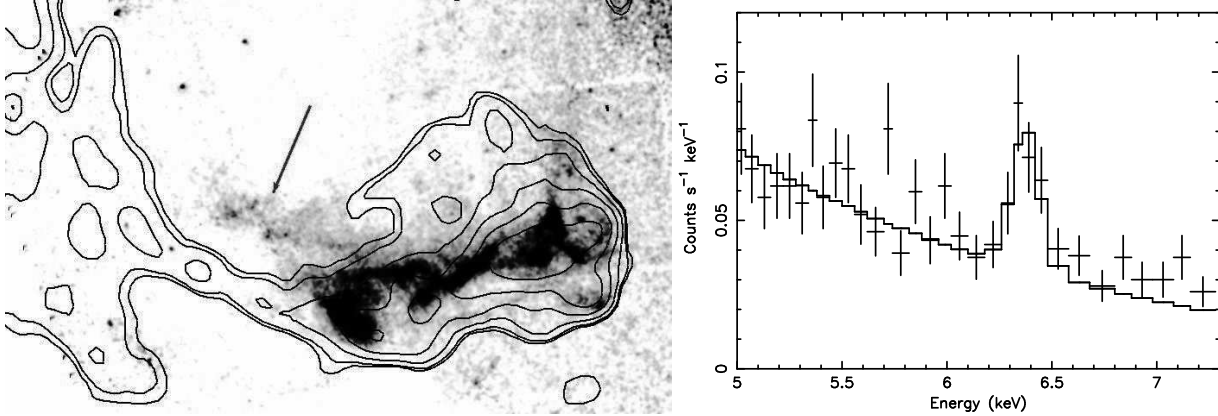


Figure 7. *XMM-Newton* image in the X-ray 2-7 keV band, which is dominated by continuum emission (left), and has totally different morphology than in softer X-ray bands. Radio contours are overlaid. The arrow indicates a region of strong X-ray continuum without obvious radio synchrotron emission. The region that emits hard X-ray continuum also emits Fe-K emission at 6.4 keV (right) [63,64,54].

has consequences for the mass estimates [15]. The discovery of X-ray synchrotron radiation from shell-type remnants have complicated the analysis of their X-ray emission, but has given unexpected new insights in the particle acceleration properties of supernova remnants.

These advances in our understanding have been made possible by the emergence of spatially resolved X-ray spectroscopy, first with *ASCA* and *BepoSAX*, and now fruitfully continued with *Chandra* and *XMM-Newton*.

I thank Kurt van der Heyden for generating Fig. 4. This work was supported by NASA's Chandra Postdoctoral Fellowship Award No. PF0-10011 issued by the Chandra X-ray Observatory Center, which is operated by the SAO under NASA contract NAS8-39073.

REFERENCES

1. K. Koyama et al., *Nat* 378 (1995) 255.
2. S.E. Woosley and T.A. Weaver, *ApJS* 101 (1995) 181.
3. K. Nomoto et al., *Nucl. Phys. A* 621 (1997) 467.
4. S.P. Reynolds and J.W. Keohane, *ApJ* 525 (1999) 368.
5. J.L. Tonry et al., *ApJ* 594 (2003) 1.
6. K.Z. Stanek et al., *ApJL* 591 (2003) L17.
7. D. Branch et al., *PASP* 107 (1995) 1019.
8. B. Aschenbach, R. Egger and J. Trumper, *Nat* 373 (1995) 587.
9. E. Miyata et al., *PASJ* 50 (1998) 257.
10. A. Heger et al., *ApJ* 591 (2003) 288.
11. F. Camilo et al., *ApJL* 567 (2002) L71.
12. G.G. Pavlov et al., *ApJL* 569 (2002) L95.
13. M. Gonzalez and S. Safi-Harb, *ApJL* 583 (2003) L91.
14. J. Vink, *New Astronomy Reviews* in press, (astro-ph/0310518) (2004).
15. F. Favata et al., *A&A* 324 (1997) L49.
16. J. Vink et al., *A&A* 344 (1999) 289.
17. J. Vink et al., *AdSpR25* (2000) 689.
18. M.C. Maccarone, T. Mineo and A. Preite-Martinez, *A&A* 368 (2001) 267.
19. J. Vink et al., *ApJL* 560 (2001) L79.
20. J.P. Hughes et al., *ApJL* 528 (2000) L109.
21. U. Hwang and J.M. Laming, *ApJ* 597 (2003) 362.
22. R. Willingale et al., *A&A* 381 (2002) 1039.
23. E.V. Gotthelf et al., *ApJL* 552 (2001) L39.
24. K.A. Flanagan et al., *Young Supernova Remnants: AIP Conf. Proc.*, Vol. 565. College Park, 226–229, 2001.
25. A.I. MacFadyen, (2003), astro-ph/0301425.
26. K. Kifonidis et al., *A&A* 408 (2003) 621.

27. D. Arnett, *Supernovae and Nucleosynthesis* (NJ: Princeton Univ. Press, 1996).

28. A.F. Iyudin et al., *A&A* 284 (1994) L1.

29. A.F. Iyudin et al., *Nat* 396 (1998) 142.

30. L.S. The et al., *A&AS* 120 (1996) C357+.

31. R.E. Rothschild et al., *Nucl. Phys. B* 69 (1999) 68.

32. J. Vink and J.M. Laming, *ApJ* 584 (2003) 758.

33. J.E. Reed et al., *ApJ* 440 (1995) 706.

34. J.M. Laming and U. Hwang, *ApJ* 597 (2003) 347.

35. J. Vink, J.S. Kaastra and J.A.M. Bleeker, *A&A* 307 (1996) L41.

36. R. Willingale et al., *A&A* 398 (2003) 1021.

37. J.P. Hughes et al., *ApJL* 582 (2003) L95.

38. K.J. van der Heyden et al., *A&A* 406 (2003) 141.

39. J.P. Hughes et al., *ApJL* 444 (1995) L81.

40. R. Bandiera and S. van den Bergh, *ApJ* 374 (1991) 186.

41. U. Hwang and E.V. Gotthelf, *ApJ* 475 (1997) 665.

42. U. Hwang et al., *ApJ* 581 (2002) 1101.

43. K.K. Dyer et al., *ApJ* 551 (2001) 439.

44. K.S. Long et al., *ApJ* 586 (2003) 1162.

45. J. Vink et al., *ApJL* 587 (2003) 31.

46. A.J.S. Hamilton et al., *ApJ* 481 (1997) 838.

47. J.M. Laming et al., *ApJ* 472 (1996) 267.

48. C.E. Rakowski, P. Ghavamian and J.P. Hughes, *ApJ* 590 (2003) 846.

49. J.P. Hughes, C.E. Rakowski and A. Decourchelle, *ApJL* 543 (2000) L61.

50. T.T. Tanimori et al., *ApJL* 497 (1998) L25+.

51. A. Aharonian, F. Akhperjanian et al., *A&A* 370 (2001) 112.

52. R. Enomoto et al., *Nat* 416 (2002) 823.

53. G.E. Allen, R. Petre and E.V. Gotthelf, *ApJ* 558 (2001) 739.

54. J. Rho et al., *ApJ* 581 (2002) 1116.

55. K. Koyama et al., *PASJ* 49 (1997) L7.

56. P. Slane et al., *ApJ* 525 (1999) 357.

57. P. Slane et al., *ApJ* 548 (2001) 814.

58. E.G. Berezhko, L.T. Ksenofontov and H.J. Völk, *A&A* 395 (2002) 943.

59. A. Bamba et al., *ApJ* 589 (2003) 827.

60. J. Vink et al., *A&A* 339 (1998) 201.

61. T. Delaney and L. Rudnick, *ApJ* 589 (2003) 818.

62. E.G. Berezhko, L.T. Ksenofontov and H.J. Völk, *A&A* in press, astro-ph/0310862.

63. J. Vink, J.S. Kaastra and J.A.M. Bleeker, *A&A* 328 (1997) 628.

64. J. Vink et al., astro-ph/0202210 (2002).

65. G.E. Allen et al., *ApJL* 487 (1997) L97.

66. J.M. Laming, *ApJ* 563 (2001) 828.

67. F. Bocchino et al., *A&A* 360 (2000) 671.

68. F. Bocchino and A.M. Bykov, *A&A* 400 (2003) 203.

69. A.M. Bykov, *A&A* 390 (2002) 327.

70. K.J. Borkowski et al., *ApJ* 550 (2001) 334.